fractal and fractional

MDPI

Article

Post Mortem Image Analysis of Astrocytes of the Human Principal Olivary Nucleus Using Geometrical and Fractal Parameters

Damjan Stojić [1,*] and Dragana Radošević [2]

[1] Laboratory of Image Analysis, Institute of Biophysics, University of Belgrade-Faculty of Medicine, 11000 Belgrade, Serbia
[2] Laboratory of Neuroanatomy, Department of Anatomy, School of Medicine, University of Novi Sad, 21137 Novi Sad, Serbia
* Correspondence: damjan.stojic@med.bg.ac.rs; Tel.: +38-11-1360-7161

Abstract: Based on their morphology, the most abundant cells within the nervous tissue of the central nervous system, astrocytes, can be divided into two types, protoplasmic astrocytes and fibrous astrocytes. A further analysis of the brain tissue with the preserved astrocytes from the human principal olivary nucleus, based on their morphological differences with age, is successfully performed in this paper. Moreover, the images of 294 astrocytes, 148 fibrous and 146 protoplasmic, from the principal olivary nucleus were used. Applied for the first time in astrocytes image analysis, the principal component analysis was used to find the most informative parameters among geometrical and fractal in each of the four predefined groups, i.e., categories, of the morphological measurements of astrocytes in the images. The proposed subsets representing different morphological features can be used to distinguish astrocyte subtypes and predict their changes during normal aging. The values of the adequated parameters in different subsets were compared between the fibrous and protoplasmic astrocytes and correlated with age. Significant differences ($p < 0.05$) between the two subtypes were found in four Euclidean and four monofractal parameters. In addition, significant correlations were found between selected parameters and the age of subjects. In the upcoming iterations of this procedure, possible refinement and upgrades are expected.

Keywords: astrocyte; morphology; monofractal; principal component analysis; aging

Citation: Stojić, D.; Radošević, D. Post Mortem Image Analysis of Astrocytes of the Human Principal Olivary Nucleus Using Geometrical and Fractal Parameters. *Fractal Fract.* **2023**, *7*, 6. https://doi.org/10.3390/fractalfract7010006

Academic Editors: Frigyes Samuel Racz, Peter Mukli, Alexander J Bies and António Lopes

Received: 26 September 2022
Revised: 1 December 2022
Accepted: 9 December 2022
Published: 21 December 2022

1. Introduction

The principal olivary nucleus (PON) is a part of the inferior olivary nuclei (ION) in the human central nervous system (CNS) that serves as a relay station between the spine and cerebellum and provides feedback to cerebellar neurons by integrating motor and sensory information [1]. The neuronal architecture of PON is built of principal neurons and a small fraction of interneurons [2] while supporting glial infrastructure contains oligodendrocytes, two types of astrocytes (protoplasmic and fibrous) [3] and microglia. However, the precise abundance of glial cell types in PON is difficult to obtain because of the limitations of the present glial markers. As a rough estimate, one can use data for the neocortex, which consists of ~20–40% astrocytes, ~50–70% oligodendrocytes and ~5–10% of microglia [4].

For the most abundant cell type in CNS, astrocytes, our previous qualitative investigations [5] postulated a small star-shaped body with many extensions of different lengths and thicknesses [6]. As in the rest of CNS, PON astrocyte subtypes are, by specificities of their physiology and morphology, closely "tuned" to serve the needs of local neurons. In this sense, protoplasmic and fibrous astrocytes of PON can be easily distinguished based on major features [7], and the assessment of their subtle morphological characteristics should rely on mathematical techniques for the analysis of morphology.

The reliable method for assessment of subtle characteristics of astrocyte morphology potentially can be implemented in the evaluation of the morphological parameters of glial cells from post-mortem specimens taken from patients that suffered from pathologies affecting PON directly (such as hypertrophic olivary degeneration) or indirectly (for example, spinocerebellar ataxia, induce retrograde neuronal degeneration in ION [8]). This application could help reveal such changes in Alzheimer's disease for which, despite a decrease in the number of neurons and oligodendrocytes, no changes in ION astrocyte number were found following Lasn et al. [9]. Since neurodegenerative diseases are frequently accompanied by changes in the morphology of astrocytes [10], it is more than probable that such changes occur in PON in Alzheimer's disease, as well as in normal aging. However, the changes in morphology and number of astrocytes in these pathologies, as well as their possible role in the pathogenesis of these diseases, were largely overlooked and the exact morphological classification of the underlying structure is one of the first steps.

The scope of this study was to employ fractal analysis to distinguish protoplasmic and fibrous astrocytes in PON and assess the Euclidean and monofractal parameters that appropriately describe the changes in their morphology during normal aging. This study also gives an extension of the procedure exposed in our previous work with neurons, which is now applied to glial cells and can be regarded as the widening of the proposed image analysis technique.

2. Materials and Methods

2.1. Histological Procedure and Images Preparation

The material used in this study, i.e., brain samples, originates from 30 cadavers (20 males and 10 females) and belongs to the Department of Anatomy, Medical faculty of the University of Novi Sad. All cadavers from whom the specimens of PON were taken were subjects of standard autopsies that did not report any signs of neurological diseases or acute cerebrovascular injuries or diseases and were between the ages of 40 to 90 years. The study on this material was approved by the ethics committee (01-3367/1) for detailed examination. The samples were from bilateral sections of the human PON, and all the samples were carved into 2 cm $\times$ 1.25 cm, which approximately corresponds to the PON dimensions suitable for a treatment with a modified Golgi method of silver impregnation by Kopsch-Bubenaite [11]. Tissue samples with the dimension of PON were cut on a sliding microtome in a horizontal plane relative to the anatomical position of the PON with a thickness of 70 μm. In a publication [12], the whole procedure is explained in detail.

Tissue parts are analyzed with an optical microscope "Leica DC 100" (Leica Microsystems, Wetzlar, Germany) with a magnification of 400$\times$ [13]. Digital images of glial cells are captured and transferred using the corresponding software "Digital Camera System" (Leica Microsystems, Hererbrugg, Switzerland). Glial cell pictures are recovered by analyzing several images from 3 to 12 in one set [13,14]. A particular image of the cross-section is gathered as a color image and saved in the TIFF format. The whole procedure is described in the paper [12] with accompanying descriptive images and is given in the paragraph below.

The image manipulation was performed as follows. The digitalized horizontal cross-sections were loaded in the Image J editor (http://rsbweb.nih.gov/ij, accessed on 10 February 2022), National Institute of Health, Bethesda, MD, USA), and by a skilled, experienced anatomist, alternations of an image with Image J tools were made. Inside the Image J GUI environment, tools were used for merging multiple different images into a single image of an astrocyte. Next, the image was converted into grayscale [13] and afterward, in binary format, within the menu option "Threshold", modification of the image was made. The specialists reconstructed the shape of the soma and each feeler (extension) and removed all the remains of artifacts with the Image J tools. Thus, the investigated sample consisted of 294 binary images of the human PON astrocytes, 148 of the fibrous type and 146 of the protoplasmic type. In the Figure 1. below, the optical slice cross-section of fibrous (left, first image line) and protoplasmic (second image line) astrocytes in PON are given and their attributed (right) binary images.

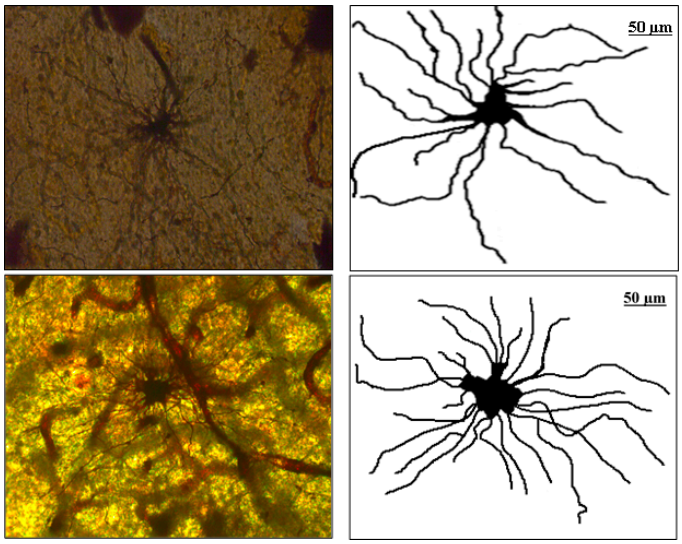

Figure 1. First image line: Optical slice cross-section of fibrous astrocyte in PON and attributed (right) binary image. Second image line: Optical slice cross-section of protoplasmic astrocyte in PON and attributed (right) binary image.

2.2. Analyzed Parameters

The main goal of this study was to use chosen parameters to elucidate through different categories which horizontal projection in the image is better for description since it exhibits a greater amount of sustainable variation in our given sample of images and has remarkable evolution during maturation and aging period. Using just one parameter from each group (i.e., category), fibrous and protoplasmic astrocyte morphology and their evolution were described. The initial number of parameters was 18 (Euclidean and monofractal) and classified into four groups: size, shape, complexity and homogeneity. The 18 proposed parameters were reduced to 15 (as three of those parameters were characterized as redundant, explicitly, the group shape was reduced from 6 parameters to 3) as principal component analysis (PCA) revealed similarities in this category. From each group, one parameter was chosen as it was the most descriptive, and the aging process was followed. The selection relied on both a variance and a standard deviation (SD) (although they are related by simple mathematical expression) since different interpretations allow underlining subtle differences in certain steps in the process.

The parameters used in this study to describe morphology were fifteen parameters that quantified four properties, i.e., groups. These parameters were calculated using the box-counting method [15–18], either by an option in Image J ("Fractal Box count") or by the FracLac plugin in the Image J software [19].

The selected parameters for the complete procedure were reduced to the optimal number for examination via PCA. This procedure rotates the observed coordinate frame of the initial set of parameters in its own space of parameters so that they are sorted in a manner of decreasing variance. These are the principal components. The examinator can now observe which of them (in the given subset) has the greatest influence and, with the aid of supplementary PCA tools in different categories, deduce their individual correspondence. Since the various principal components combinations can mask the best ones, the investigator can decide which one is the best for the description of the corresponding subset. The whole procedure was first presented by Carl Pearson in 1901 [20] and is explained in detail in a relatively novel paper [21].

Euclidean parameters used in 2D projections were parameters characterizing the area of the soma (A_s), the area of the glial field (A_{gf}) and the area of the receptive field (A_{rf}). Furthermore, the glial field perimeter (P_{gf}) parameter, the circularity of the glial field (M_{gf}), the number of intersections of feelers (N) and the maximal number of intersections of feelers (N_m) were used as descriptive parameters for the glial shape. In addition, chosen

monofractal parameters were binary parameters that quantified the fractal dimension of the soma ($(D_{bin})_s$), glial cells ($(D_{bin})_g$) and glial field ($(D_{bin})_{gf}$) in those images. Similarly, the parameter of fractal dimension ($(D_{out})_{gf}$) of the glial field that quantified the one-pixel broad outline image border of the glial field and the fractal dimension of the skeletonized fractal image of the astrocyte ($(D_{skel})_g$) were engaged, as well as a family of fractal parameters such as lacunarity of the soma (L_s), glia (L_g) and glial field (L_{gf}). All monofractal parameters were calculated either from a binary image of the glial soma or the glia [22], and a skeleton image for a skeletonized parameter was estimated when all extensions were reduced to a single-pixel wide line in Image J through the "Process-Binary-Skeletonize" [23] menu option.

2.3. Statistical Analysis and Tools

This paper has investigated the difference between cell types with a two-tailed t-test for independent samples. Shapiro–Wilk and Chi-square tests were performed to check conditions of normality and homogeneity that are prerequisites for application of ANOVA and the statistical significance between groups was examined by one-way ANOVA with a Bonferroni post hoc test [24]. A value of $p < 0.05$ was considered statistically significant. The statistics in the Tables are implemented with free R version 4.2.2, and so were all PCA-related calculations [25].

3. Results

3.1. PCA and the Selection of Parameters

As shown in the previous Section 2.1, this study used eighteen parameters (Euclidean and monofractal) that quantified four properties of the 2D image (size, shape, complexity and homogeneity), in this case, the horizontal projection of astrocytes.

(A) Size

This class consisted of three Euclidean parameters of the soma, the area of the soma (A_s), the glial field (A_{gf}) and the receptive field (A_{rf}). In addition, three monofractal parameters of the soma, binary fractal soma dimension ($(D_{bin})_s$), glial cells binary fractal dimension ($(D_{bin})_g$) and glial field binary fractal dimension ($(D_{bin})_{gf}$) were incorporated. After the PCA was performed, the greatest contribution came from the first two principal components (Table 1).

Table 1. The importance of the 15 parameters of astrocytes presented in the basis of principal components. First, reduction to only one parameter was carried out by the examination of variance (v) and standard deviation (SD). Afterward, a final conclusion was drawn analyzing the scree plot and bi-plot.

Property	Parameters	Component	v	SD
Size	A_s, A_{gf}, A_{rf}, $(D_{bin})_s$, $(D_{bin})_g$ and $(D_{bin})_{gf}$	First	2.4	1.6
		Second	1.3	1.1
		Third	1	1
		Fourth	0.8	0.9
		Fifth	0.6	0.7
		Sixth	0	0
Shape	P_{gf}, M_{gf} and $(D_{out})_{gf}$	First	1.2	1.1
		Second	1	1
		Third	0.8	0.9
Complexity	N, N_m and $(D_{skel})_g$	First	1.9	1.4
		Second	0.7	0.9
		Third	0.4	0.6
Homogeneity	L_s, L_g and L_{gf}	First	1.3	1.1
		Second	1	1
		Third	0.8	0.9

In the scree plot (SP), the main contribution came from the first two components (Figure 2), and the SD (Table 1, values above 1) confirmed such a conclusion. Furthermore, the ν (i.e., eigenvalues of the correlation matrix) was greater than one for the first two principal components. The corresponding standardized bi-plot was performed in order to find which component had the best influence on the original parameters. In this case (Figure 3), the A_{rf} and A_{gf} had the greatest variability along the first principal component and were pointed in the same direction. However, the As was selected as it involves variability in both principal components. This parameter also makes visual comprehension of size parameters more understandable.

(B) Shape

In this class, we encountered five Euclidean parameters (P_{gf}, M_g, R_{gf}, A_{rgf} and S_{gf}) and one monofractal parameter ($(D_{out})_{gf}$) of the glial field. The initial PCA, generated from six parameters, indicated the possibility of the reduction and the novel scree plot is presented (Figure 4). Specifically, the new bi-plot (Figure 5) conserved projection orientation on the first two principal components and new vectors had higher weighting than the previous ones. Therefore, the PCA has reduced the parameters of the shape to the three relevant: P_{gf}, M_{gf} and $(D_{out})_{gf}$. The new PCA (from three parameters) indicated that only one principal component had ν and SD above one (Table 1), and the P_{gf} had the greatest positive influence on the first two principal components (Figure 5).

(C) Complexity

In this group, two Euclidean (N and N_m) and one monofractal ($(D_{skel})_g$) parameters of astrocytes were used. Following PCA, only one principal component was relevant (Table 1, the ν and SD above one, or see Figure 6), and after the bi-plot (Figure 7), N was the most important parameter in this class. It depended equally on the first two principal components, i.e., it had equal projections of variability.

(D) Homogeneity

Three monofractal, i.e., lacunarity, parameters of the soma (L_s), glia (L_g) and glial field (L_{gf}) quantified this property. Following PCA, the first principal component had ν and SD above one (Table 1, Figure 8), and the corresponding bi-plot (Figure 9) suggested L_g as the parameter that had an important contribution to the first two principal components.

Concerning scree plots in the graphs below, variance interpretation was given in arbitrary units (a. u.), as in different groups, mixing different in nature parameters (geometric and fractal) was necessary. In the bi-plots figures below, fibrous (F) and protoplasmic (P) astrocytes at corresponding parameter spaces are denoted. Since authors are unable to find any patent concerning how ether fibrous or protoplasmic astrocytes are distributed, we can say that the distribution of types of astrocytes can be regarded as homogeneous and isotropic.

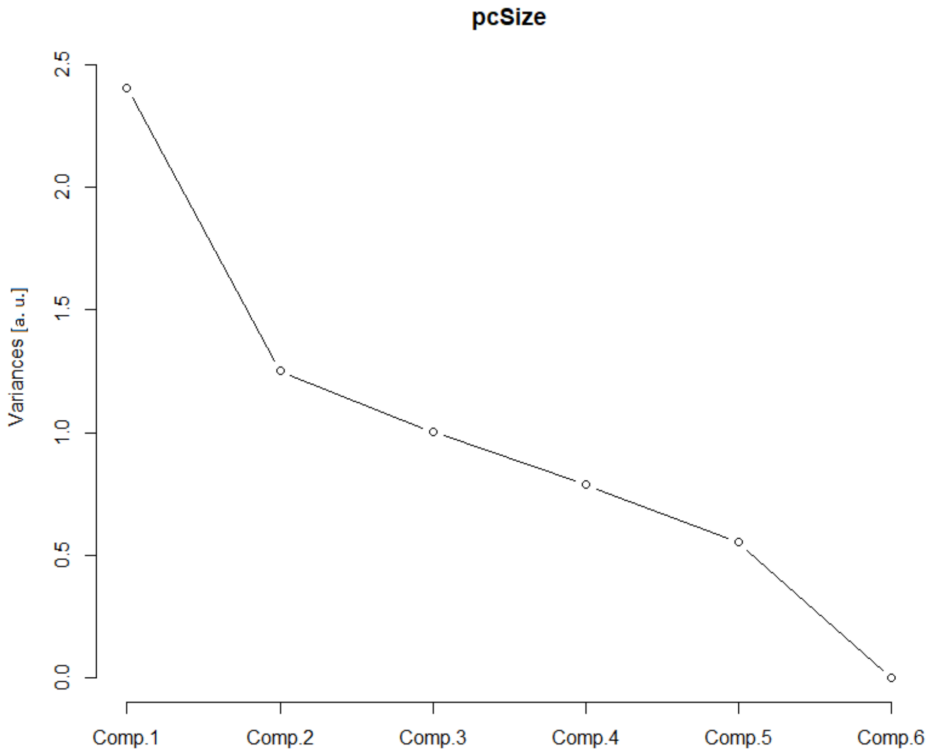

Figure 2. Size scree plot. The relationship between the variances (eigenvalues) and principal components for the size for the analyzed sample of astrocytes in the given group.

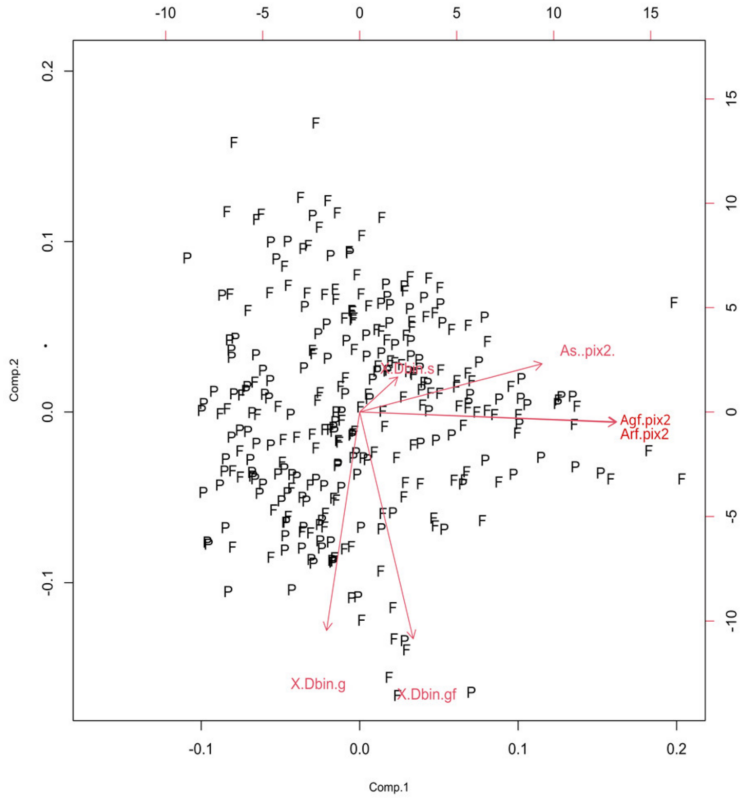

Figure 3. The PCA-based bi-plots of parameters characterizing morphological features in the given parameter space. Relationships between first two standardized principal components of the size.

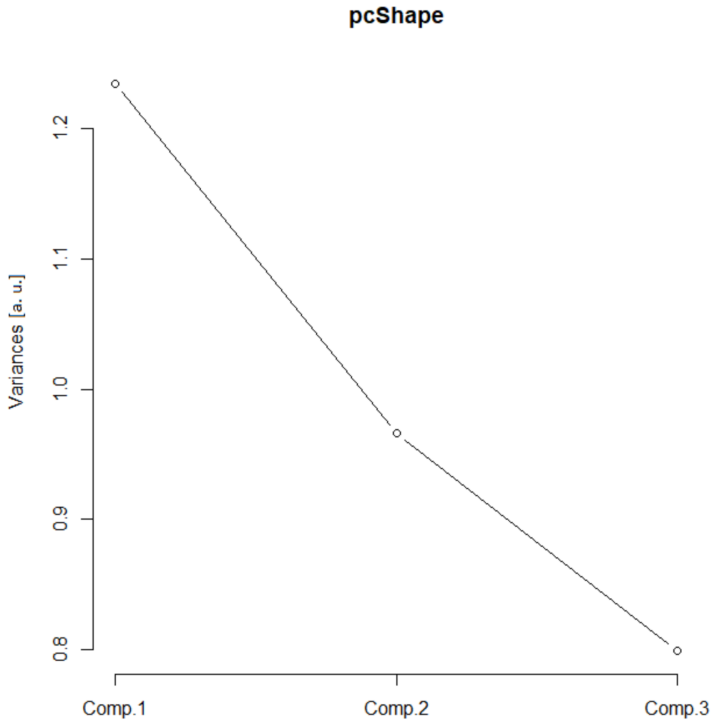

Figure 4. Shape scree plot. The relationship between the variances (eigenvalues) and principal components for the shape for the analyzed sample of astrocytes in the given group.

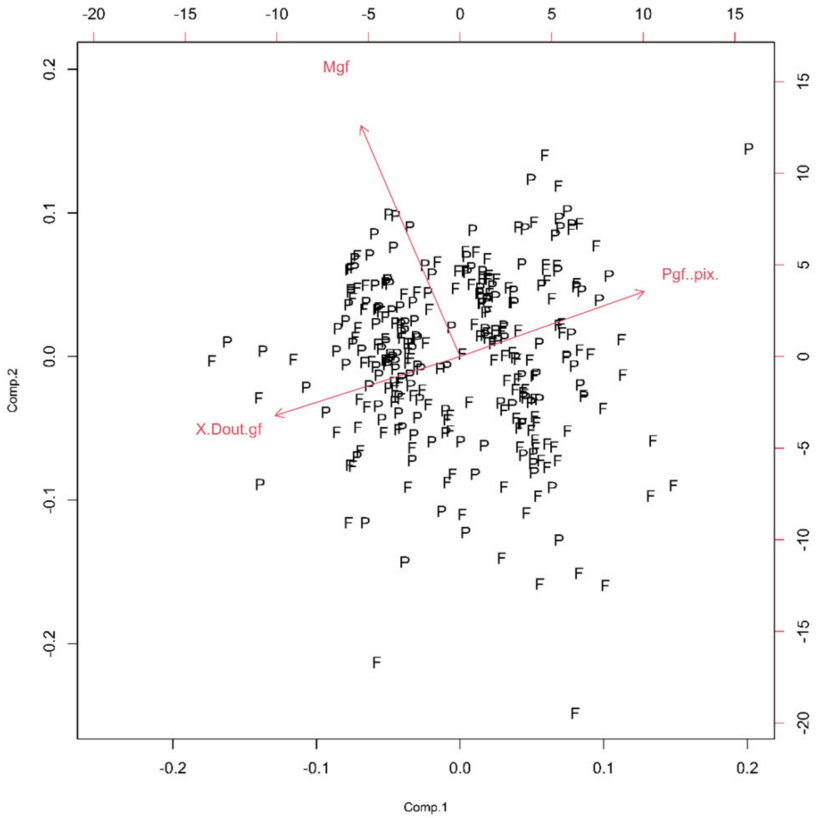

Figure 5. The PCA-based bi-plots of parameters characterizing morphological features in the given parameter space. Relationships between the first two standardized principal components of the shape.

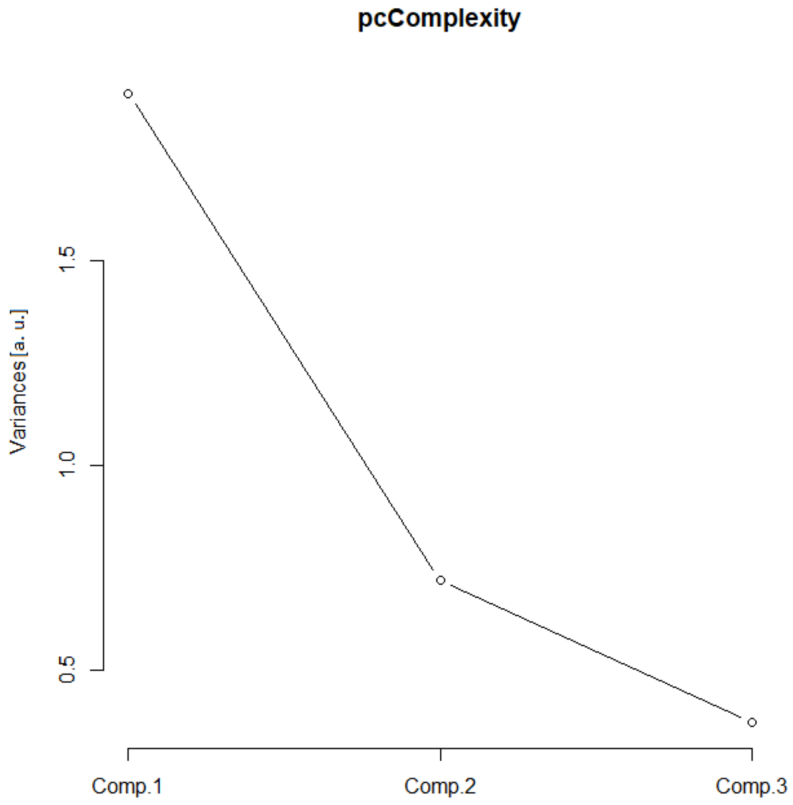

Figure 6. Complexity scree plot. The relationship between the variances (eigenvalues) and principal components for the complexity of the analyzed sample of astrocytes in the given group.

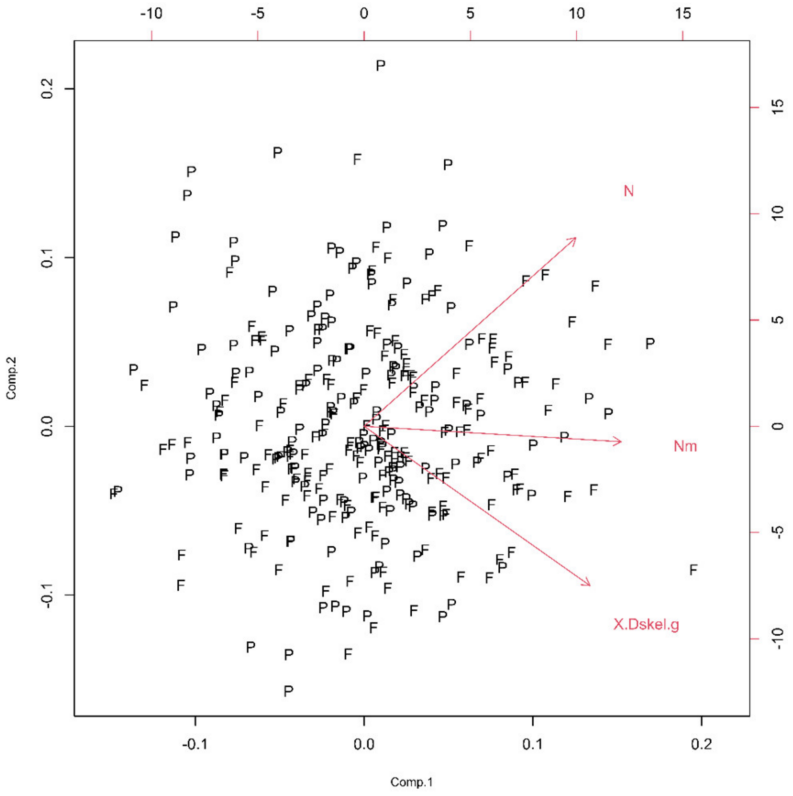

Figure 7. The PCA-based bi-plots of parameters characterizing morphological features in the given parameter space. Relationships between first two standardized principal components of the complexity.

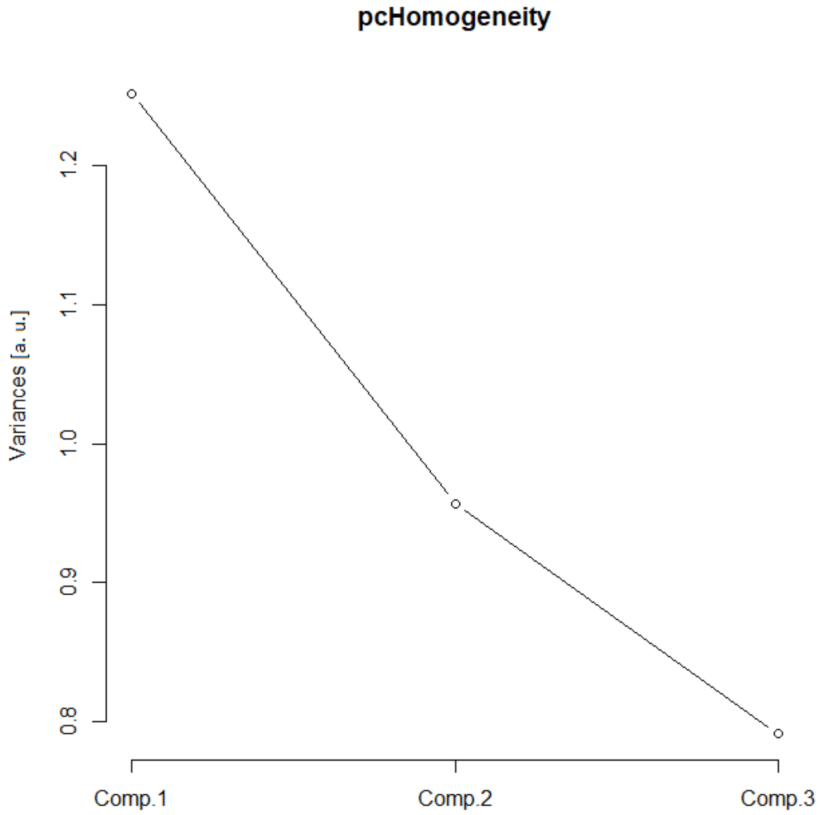

Figure 8. Homogeneity scree plot. The relationship between the variances (eigenvalues) and principal components for the homogeneity for the analyzed sample of astrocytes in the given group.

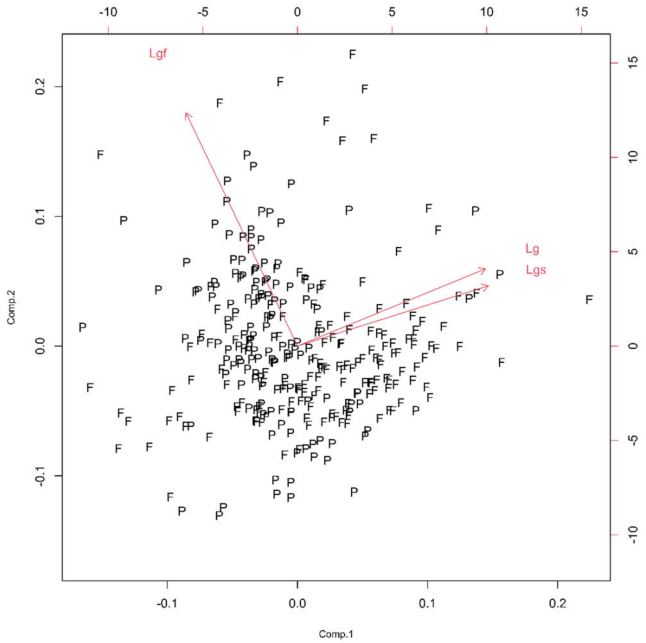

Figure 9. The PCA-based bi-plots of parameters characterizing morphological features in the given parameter space. Relationships between first two standardized principal components of the homogeneity. A careful reader should have in mind that the notation in the given graph in this group consists of *Lgf*, *Lg* and *Lgs*, and in the text, of corresponding *Lgf*, *Lg* and *Ls*, respectfully.

3.2. Quantitative Analysis of Types

The examined sample (294 images) consisted of two types of astrocytes: fibrous (148 images) and protoplasmic (146 images). The morphology was quantified by determining fifteen parameters (Table 2, below) according to Section 3.1, where six parameters of the shape were reduced to three. The table shows the mean values (and standard errors) between two types of astrocytes: the four most important parameters (A_s, P_{gf}, N and L_g) are marked in bold. The last column shows the level of significance (p), and significant differences between the two types are bolded.

Table 2. The mean values and standard errors of fifteen parameters of the size (A_s, A_{gf}, A_{rf}, $(D_{bin})_s$, $(D_{bin})_g$ and $(D_{bin})_{gf}$), the shape (P_{gf}, M_{gf} and $(D_{out})_{gf}$), the complexity (N, N_m and $(D_{skel})_g$) and the homogeneity (L_s, L_g and L_{gf}) of two types of astrocytes. The comparison of means between two independent samples was presented with the p value, while statistical significance was bolded.

Property	Parameter	Fibrous	Protoplasmic	p
Size	**A_s ($\times 10^3$ pix^2)**	**8.8 ± 0.3**	**6.6 ± 0.2**	**<0.01**
	A_{gf} ($\times 10^5$ pix^2)	5.9 ± 0.2	4.9 ± 0.2	**0.04**
	A_{rf} ($\times 10^5$ pix^2)	5.8 ± 0.2	4.8 ±0.2	**0.05 ***
	$(D_{bin})_s$	1.723 ± 0.006	1.745 ± 0.006	0.08
	$(D_{bin})_g$	1.425 ± 0.003	1.437 ± 0.003	0.1
	$(D_{bin})_{gf}$	1.816 ± 0.004	1.818 ± 0.003	0.73
Shape	**P_{gf} ($\times 10^3$ pix)**	**3.20 ± 0.06**	**2.83 ± 0.07**	**<0.01**
	M_{gf} (pix)	0.703 ± 0.006	0.713 ± 0.005	0.24
	$(D_{out})_{gf}$	1.062 ± 0.002	1.064 ± 0.002	0.44
Complexity	**N**	**6.9 ± 0.1**	**7.0 ± 0.1**	0.68
	N_m	14.1 ± 0.3	14.4 ±0.2	0.38
	$(D_{skel})_g$	1.169 ± 0.003	1.150 ± 0.004	**<0.01**
Homogeneity	L_s	0.125 ± 0.003	0.119 ± 0.002	**<0.01**
	L_g	**0.623 ± 0.008**	**0.588 ± 0.005**	**<0.01**
	L_{gf}	$0.123^{\#1}$ ± 0.001	$0.123^{\#4}$ ± 0.001	**<0.01**

Significant difference at $p < 0.05$, * border case, # the difference was made at the 4th decimal number and showed that the value is slightly higher for protoplasmic than for fibrous astrocytes.

The morphological characteristics of fibrous astrocytes generally had higher mean values than protoplasmic ones (Table 2). This was particularly evident in the case of Euclidean (A_s, A_{gf}, A_{rf} and P_{gf}) and monofractal ($(D_{skel})_g$ and L_g) parameters. However, this conclusion was the opposite for M_{gf}, $(D_{bin})_s$, $(D_{bin})_g$, $(D_{bin})_{gf}$ and L_{gf}. Furthermore, the $(D_{out})_{gf}$ had approximately the same mean in both types. Finally, the two types differed significantly through eight quantitative parameters (Table 2, bold letters) or in all four morphological properties. However, it should be noted that the result for pairs A_{gf}–A_{rf} and L_s–L_g was no surprise, as Figures 3 and 9 clearly showed that they are dependent.

The four most important parameters (A_s, P_{gf}, N and L_g) were emphasized in Table 3 in the next paragraph.

3.3. Age Dependence of Parameters Describing the Morphology

The results of the Pearson correlation test (see Table 3) on parameters suggest that A_s decreases with age, which can primarily be attributed to the age-related shrinking of the soma of the fibrous astrocytes. Almost identical correlation coefficients were observed for L_g, which suggests that the two parameters give the same information concerning age dependence. The P_{gf} parameter also decreases with age, again dominantly for fibrous astrocytes. Parameter N does not show any age dependence. Although it was not selected

by PCA analysis, $(D_{skel})_g$ exhibits a negative correlation with age that now can be attributed to a decrease in this parameter for protoplasmic astrocytes.

In our last overview (Table 4), by the given parameter, the mean values with standard errors of two types of astrocytes are outlined. The higher means in Age Group 1 for both types of astrocytes were valid only in the case of the Euclidean parameter of the cell size. However, Table 4 clearly shows the existence of morphological differences between groups: six parameters in fibrous and three in protoplasmic astrocytes.

Table 3. The Pearson correlation coefficients between the selected parameters and age.

Parameter	Total PON Astrocytes	Fibrous	Protoplasmic
A_s	−0.53 ***	−0.61 **	−0.29
P_{gf}	−0.33 *	−0.56 **	−0.07
N	0.03	0.13	−0.09
L_g	−0.53 ***	−0.60 **	−0.25
$(D_{skel})_g$	−0.41 **	0.1	−0.75 ***

* $p < 0.05$, ** $p < 0.01$, *** $p < 0.001$.

Table 4. The mean values (standard errors) between second groups of maturation (Age Group 1) and aging (Age Group 2) in fibrous and protoplasmic astrocytes. Column p shows a statistical estimate of the differences between the groups.

Property	Parameter	Fibrous		p	Protoplasmic		p
		Age Group 1	Age Group 2		Age Group 1	Age Group 2	
Size	A_s ($\times 10^3$ pix^2)	9.8 ± 0.7	7.5 ± 0.4	< 0.01	8.0 ± 0.4	6.6 ± 0.3	< 0.01
	A_{gf} ($\times 10^5$ pix^2)	6.5 ± 0.3	5.2 ± 0.3	< 0.01	6.0 ± 0.4	5.3 ± 0.4	0.2
	A_{rf} ($\times 10^5$ pix^2)	6.4 ± 0.3	5.2 ± 0.3	< 0.01	6.0 ± 0.4	5.3 ± 0.4	0.207
	$(D_{bin})_s$	1.719 ± 0.009	1.747 ± 0.009	0.03	1.74 ± 0.01	1.753 ± 0.009	0.23
	$(D_{bin})_g$	1.427 ± 0.004	1.432 ± 0.006	0.473	1.427 ± 0.005	1.430 ± 0.005	0.627
	$(D_{bin})_{gf}$	1.816 ± 0.006	1.820 ± 0.007	0.696	1.825 ± 0.007	1.820 ± 0.006	0.589
Shape	P_{gf} ($\times 10^3$ pix)	3.4 ± 0.1	3.0 ± 0.1	< 0.01	2.5 ± 0.1	2.9 ± 0.1	0.086
	M_{gf} (pix)	0.71 ± 0.01	0.70 ± 0.01	0.694	0.726 ± 0.008	0.717 ± 0.009	0.461
	$(D_{out})_{gf}$	1.061 ± 0.003	1.066 ± 0.007	0.202	1.063 ± 0.003	1.063 ± 0.003	0.957
Complexity	N	6.9 ± 0.2	7.4 ± 0.2	0.107	7.1 ± 0.2	6.9 ± 0.2	0.296
	N_m	14.2 ± 0.4	15.1 ± 0.5	0.146	14.6 ± 0.5	13.9 ± 0.4	0.24
	$(D_{skel})_g$	1.167 ± 0.004	1.176 ± 0.006	0.245	1.177 ± 0.004	1.097 ± 0.004	< 0.001
Homogeneity	L_s	0.134 ± 0.004	0.133 ± 0.005	0.799	0.121 ± 0.005	0.108 ± 0.003	0.027
	L_g	0.67 ± 0.01	0.61 ± 0.01	< 0.001	0.607 ± 0.007	0.589 ± 0.009	0.104
	L_{gf}	0.115 ± 0.005	0.108 ± 0.003	0.183	0.133 ± 0.005	0.136 ± 0.005	0.73

Statistical significance at $p < 0.05$.

4. Discussion

The Euclidean and fractal parameters used in this study are suitable for highlighting different morphological aspects of astrocytes from the human PON. All fractal parameters

were monofractal and obtained by calculating monofractal parameters on each 2D image of the astrocyte using the box-counting technique [15,18].

The astrocytes, in general, are a class of glial cells that sustain homeostasis and provide defense for CNS, and with a large variety of functions, they demonstrate remarkable adaptive plasticity that presents current functional maintenance and the optimal evolution during the development and aging [15]. Fibrous astrocytes populate the brain's white matter, the spinal cord, the optic nerve, and the nerve fiber of the retina and show a diverse morphology [15]. Protoplasmic astrocytes, on the other hand, are dominantly found in the brain cortex and spinal cord gray matter and differ within anatomical structure [15]. Previous qualitative studies investigated the number of primary extensions, their direction and branching, but did not establish observable differences between types [5]. Results of our previous work [12] showed the differences among the astrocytes, and with this technique, this study represents an extension of the analysis to the astrocyte populations of our previous work with neurons and PCA.

To our knowledge, this is the first time that a combination of PCA and fractal analysis has been used in the characterization of the morphology of astrocytes and distinguishing their subtypes. The results may serve as an initial point in the quantitative assessment of the differences in the morphology of astrocyte subtypes that occur during some brain diseases. Furthermore, they could give an insight into the role that astrocytes have in PON in diseases of the cerebellum and other related structures.

Based on a simplified geometric analysis of the image and following the given means (Table 4) of the size group, one can conclude that protoplasmic astrocytes have a shape closer to an ellipse than the fibrous ones. On the other hand, following the meaning of fractal parameters $(D_{skel})_g$ and L_g, it is easy to conclude that fibrous astrocytes have greater curvature of the extensions and space compared to protoplasmic.

The results of our study suggest that values of several estimated parameters significantly differ between fibrous and protoplasmic astrocytes. This is not surprising considering the different abundance of those cells in white and grey matter, respectively, and their different roles within those tissue types. The fibrous astrocytes are responsible for the facilitation and support of myelinization by the clearance of extracellular ions and neurotransmitters and by secretion of pro-myelinating factors [26], while the protoplasmic ones are dedicated to supporting neurosynapses (a single human astrocyte may be in contact with around two million synapses [27]) and contribute to neurotransmitter, ion and energy homeostasis [28]. The area of the soma (A_s) is found to be significantly smaller in protoplasmic than in fibrous astrocytes, which agrees with previous morphological studies [27]. As a measure of the shape of astrocytes, the perimeter of the glial field (P_{gf}) also tends to be greater in protoplasmic astrocytes and tends to grow with age, and in fibrous astrocytes, it shrinks. That can be explained by the higher cell density in gray compared to white matter [29] and, hence, more limited space for extensions. The four fractal parameters that were similarly addressed in this study, one quantifying complexity $(D_{\mathrm{skel}})_g$, which showed a rise in fibrous and drop in protoplasmic astrocytes, and three quantifying astrocyte homogeneities, lacunarities of the soma (L_s), glia (L_g) and glial field (L_{gf}), also showed a drop in fibrous and protoplasmic astrocytes, except in L_{gf}, which grows in protoplasmic astrocytes. In general, the complexity parameters of fibrous astrocytes tend to grow with age and protoplasmic tend to shrink with age.

Since fibrous astrocytes can be dominantly found in white matter, the decrease in parameters that describe morphology could be connected with the age-related loss of myelin and consequent adaptation of astrocyte morphology to new conditions. This is in agreement with the results of the several studies [30,31], in which no loss but only changes in astrocyte morphology were observed.

In contrast, the negative correlation of $(D_{\mathrm{skel}})_g$ with age is dominated by a strong correlation only for protoplasmic astrocytes. The high value of the correlation coefficient and its high statistical significance suggest the high sensitivity of this parameter to changes in the PON gray matter. Since the loss of gray matter is generally faster than of white

matter, one may expect that $(D_{\text{skel}})_g$ could serve as a good marker for gray matter loss in diseases that affect PON and related structures.

Furthermore, the results of this paper are in good agreement with the presented works with astrocytes [12]. However, this parameter image morphology analysis field is only beginning to reveal itself. The results found in this study cannot be extended to astrocyte populations in other parts of the CNS since these morphological cell types show high dependence on cell and biochemical environment [31,32]. In this sense, the subsequent investigation and steps should search for the fortified and reliable parameters that could give us a clearer picture. Furthermore, since the analysis was performed on microscopic images obtained after a modified Golgi dying procedure, we cannot claim that similar results can be obtained if another more specific histological technique, such as GFAP treatment, is used. Therefore, this could represent another possible area for examination.

5. Conclusions

With this undergone analysis, we managed to peak in each morphological group the most suitable parameter for the description of PON astrocytes. The final aim of this kind of procedure was to find the possible different parameters in different parts of CNS that could give the possible outcomes of different stages, first, of illness-free patients and, after, of patients with neurological problems, which could be considered at the end, and similar patients with this knowledge could be, accordingly, treated.

In general, the significance of this extension was the implementation of a unifying procedure that can be used overall for examining astrocytes with minor changes in the used parameters or with no changes (i.e., the same parameters always) and obtaining the highest possible separability in each case and, thus, minimizing the influence of observer subjectivity in every case without any possibility for human error. The same objective was in our first work with neurons [14].

This paper presents a novel approach to the analysis and quantification of the images via geometrical and fractal parameters of astrocytes that involves the application of PCA analysis in the choice of parameters that adequately describe astrocyte morphology. It was shown that those parameters could help distinguish fibrous and protoplasmic astrocytes and predict changes in their morphology with age. The obtained results could serve as a basis for further research in the field of neurodegenerative diseases, which will implement this approach in assessing changes in astrocyte morphology in different age groups and in general.

Author Contributions: Conceptualization, formal analysis (PCA, fractal analysis), statistics, write draft manuscript, D.S.; collect data, histological procedure and image preparation, D.R. All authors have read and agreed to the published version of the manuscript.

Funding: This paper is partially financed by project of The Ministry of Education, Science and Technological Development No. 01-3367/1.

Institutional Review Board Statement: The study was conducted in accordance with the Declaration of Helsinki, and approved by the Ethics Committee of University of Novi Sad, Serbia (01-3367/1, 17 December 2015).

Informed Consent Statement: The brain samples were from cadavers and belonged to the histological collection of the Department of Anatomy at the University of Novi Sad, Serbia.

Data Availability Statement: Not applicable.

Acknowledgments: The authors are grateful to Dušica L. Marić (Department of Anatomy, University of Novi Sad, Serbia) for supervision in histological procedure and image editing, particularly in reconstruction of the trajectory (of the soma and each extension). Certain parts of the fractal analysis were helped and managed with the contribution of Neboša T. Milosević.

Conflicts of Interest: The authors declare no conflict of interest regarding the publication of this paper.

References

1. D'Angelo, E.; Galliano, E.; De Zeeuw, C.I. Editorial: The Olivo-Cerebellar System. *Front. Neural Circuits* **2016**, *9*, 66. [CrossRef] [PubMed]
2. Walberg, F.; Ottersen, O.P. Demonstration of GABA immunoreactive cells in the inferior olive of baboons (Papio papio and Papio anubis). *Neurosci. Lett.* **1989**, *101*, 149–155. [CrossRef] [PubMed]
3. Bozhilova-Pastirova, A.; Ovtscharoff, W. The inferior oilvary complex. *Adv. Anat. Embryol. Cell Biol.* **2000**, *155*, III-84. [CrossRef] [PubMed]
4. Verkhratsky, A.; Nedergaard, M. Physiology of Astroglia. *Physiol. Rev.* **2018**, *98*, 239–389. [CrossRef]
5. Miller, S.J. Astrocyte Heterogeneity in the Adult Central Nervous System. *Front. Cell Neurosci.* **2018**, *12*, 401. [CrossRef]
6. Radošević, D. A Morphological Analysis of the Neuronal and Glial Cells in the Human Principal Olivary Nucleus Dissertation. Ph.D. Thesis, School of Medicine, University of Novi Sad, Novi Sad, Serbia, 2019.
7. Rowitch, D.H.; Kriegstein, A.R. Developmental genetics of vertebrate glial-cell specification. *Nature* **2010**, *468*, 214–222. [CrossRef]
8. Koeppen, A.H. The pathogenesis of spinocerebellar ataxia. *Cerebellum* **2005**, *4*, 62–73. [CrossRef]
9. Lasn, H.; Winblad, B.; Bogdanovic, N. Neuroglia in the inferior olivary nucleus during normal aging and Alzheimer's disease. *J. Cell Mol. Med.* **2006**, *10*, 145–156. [CrossRef]
10. Li, K.; Li, J.; Zheng, J.; Qin, S. Reactive Astrocytes in Neurodegenerative Diseases. *Aging Dis.* **2019**, *10*, 664–675. [CrossRef]
11. Lalošević, D.; Somer, L.; Đolai, M.; Lalošević, V.; Mažibrada, J.; Krnojelac, D. *Mikroskopska Laboratorijska Tehnika u Medicine*; Medicinski Fakultet Novi Sad-WUS Austrija: Novi Sad, Serbia, 2005.
12. Stojić, D.; Radošević, D.; Rajković, N.; Milošević, N.T. 2D Images of Astrocytes in the Human Principal Olivary Nucleus: Monofractal Analysis of the Morphology. *J. Biosci. Med.* **2021**, *9*, 38–48. [CrossRef]
13. Krstonošić, B.; Milošević, N.T.; Marić, D.L.; Babović, S.S. Quantitative analysis of spiny neurons in the adult human caudate nucleus: Can it confirm the current qualitative cell classification? *Acta Neurol. Belg.* **2015**, *115*, 273–280. [CrossRef] [PubMed]
14. Stojić, D.; Radošević, D.; Rajković, N.; Marić, D.L.; Milošević, N.T. Classification by morphology of multipolar neurons of the human principal olivary nucleus. *Neurosci. Res.* **2021**, *170*, 66–75. [CrossRef] [PubMed]
15. Fernández, E.; Jelinek, H.F. Use of fractal theory in neuroscience: Methods, advantages, and potential problems. *Methods* **2001**, *24*, 309–321. [CrossRef] [PubMed]
16. Ristanović, D.; Milosević, N.T.; Jelinek, H.F.; Stefanović, I.B. Mathematical modelling of neuronal dendritic branching patterns in two dimensions: Application to retinal ganglion cells in the cat and rat. *Biol. Cybern.* **2009**, *100*, 97–108. [CrossRef] [PubMed]
17. Di Ieva, A.; Grizzi, F.; Jelinek, H.; Pellionisz, A.J.; Losa, G.A. Fractals in the Neurosciences, Part I: General Principles and Basic Neurosciences. *Neuroscientist* **2014**, *20*, 403–417. [CrossRef]
18. Milosevic, N.T. *The Morphology of Brain Neurons: Box Counting Method in Quantitative Analysis of 2D Image*; The Fractal Geometry of the Brain; Di Ieva, A., Ed.; Springer: New York, NY, USA, 2016; pp. 109–126.
19. Karperien, A. FracLac for ImageJ. Version 2.0. 2007. Available online: https://imagej.nih.gov/ij/plugins/fraclac/fraclac-manual.pdf (accessed on 10 May 2022).
20. Karl Pearson, F.R.S. LIII. On lines and planes of closest fit to systems of points in space. *Lond. Edinb. Dublin Philos. Mag. J. Sci.* **1901**, *2*, 559–572. [CrossRef]
21. Shlens, J. A Tutorial on Principal Component Analysis. Google Research, Mountain View, CA. *arXiv* **2014**, arXiv:1404.1100v1. [CrossRef]
22. Grbatinić, I.; Milošević, N. Classification of Adult Human Dentate Nucleus Border Neurons: Artificial Neural Networks and Multidimensional Approach. *J. Theor. Biol.* **2016**, *404*, 273–284. [CrossRef]
23. Rajković, N.; Krstonošić, B.; Milošević, N. Box-Counting Method of 2D Neuronal Image: Method Modification and Quantitative Analysis Demonstrated on Images from the Monkey and Human Brain. *Comput. Math. Methods Med.* **2017**, *2017*, 8967902. [CrossRef]
24. Riffenburgh, R.H. *Statistics in Medicine*; Academic Press: New York, NY, USA, 1999.
25. R Core Team. *R: A Language and Environment for Statistical Computing*; R Foundation for Statistical Computing: Vienna, Austria, 2022; Available online: https://www.R-project.org/ (accessed on 14 September 2022).
26. Lundgaard, I.; Osório, M.J.; Kress, B.T.; Sanggaard, S.; Nedergaard, M. White matter astrocytes in health and disease. *Neuroscience* **2014**, *276*, 161–173. [CrossRef]
27. Oberheim, N.A.; Takano, T.; Han, X.; He, W.; Lin, J.H.C.; Wang, F.; Xu, Q.; Wyatt, J.D.; Pilcher, W.; Ojemann, J.G.; et al. Uniquely hominid features of adult human astrocytes. *J. Neurosci.* **2009**, *29*, 3276–3287. [CrossRef] [PubMed]
28. Köhler, S.; Winkler, U.; Hirrlinger, J. Heterogeneity of Astrocytes in Grey and White Matter. *Neurochem. Res.* **2021**, *46*, 3–14. [CrossRef] [PubMed]
29. Azevedo, F.A.; Carvalho, L.R.; Grinberg, L.T.; Farfel, J.M.; Ferretti, R.E.L.; Leite, R.E.P.; Filho, W.J.; Lent, R.; Herculano-Houzel, S. Equal numbers of neuronal and nonneuronal cells make the human brain an isometrically scaled-up primate brain. *J. Comp. Neurol.* **2009**, *513*, 532–541. [CrossRef] [PubMed]
30. Lasn, H.; Winblad, B.; Bogdanovic, N. The number of neurons in the inferior olivary nucleus in Alzheimer's disease and normal aging: A stereological study using the optical fractionator. *J. Alzheimer's Dis.* **2001**, *3*, 159–168. [CrossRef] [PubMed]

31. Lasn, H.M.D. The Principal Inferior Olivary Nucleus in Aging and Alzheimer's Disease Dissertation. Ph.D. Thesis, Karolinska Institutet, Stockholm, Sweden, 2006.
32. Zhou, B.; Zuo, Y.X.; Jiang, R.T. Astrocyte morphology: Diversity, plasticity, and role in neurological diseases. *CNS Neurosci. Ther.* **2019**, *25*, 665–673. [CrossRef] [PubMed]